

A Fully Numerical Approach to One-Loop Amplitudes

M. Moretti^a F. Piccinini^b A.D. Polosa^c

^a*Dipartimento di Fisica, Università di Ferrara
Via Saragat 1, I-44100, Ferrara, Italy*

^b*Istituto Nazionale di Fisica Nucleare, Sezione di Pavia
Via A. Bassi 6, 27100, Pavia, Italy*

^c*Istituto Nazionale di Fisica Nucleare, Sezione di Roma
P.le A. Moro 2, I-00185, Roma, Italy*

Abstract

We suggest a new approach for the automatic and fully numerical evaluation of one-loop scattering amplitudes in perturbative quantum field theory. We use suitably formulated dispersion relations to perform the calculation as a convolution of tree-level amplitudes. This allows to take advantage of the iterative numerical algorithms for the evaluation of leading order matrix elements.

1 Introduction

The LHC will provide unprecedented experimental and theoretical challenges. Among others, the presence of many final state jets for any interesting observable, makes absolutely crucial a better control of theoretical predictions and in particular of higher order contributions. At present several Monte Carlo event generators based on exact Leading Order (LO) matrix elements are available such as **Alpgen** [1], **Helac** [2], **MadEvent** [3] and **Sherpa** [4]. These codes are of extreme importance for the modeling of multi-jet final states. Nevertheless, the main problem connected with LO calculations is the strong factorisation/renormalisation scale dependence. In this respect it would be useful to have also Next-to-Leading Order (NLO) calculations for such multi-jet final states in order to better control the overall normalization of the theoretical predictions. Given the huge complexity of the calculations, many theoretical efforts have been recently devoted to the development of new approaches to the problem.

The real part of the NLO corrections of any n -body final state, given by $(n+1)$ -body tree-level matrix elements, can be computed efficiently thanks to automated helicity amplitudes [5] or fully numerical algorithms [6,7], which allowed the development of the above mentioned LO matrix element event generators. On the other hand the NLO virtual corrections for a generic $2 \rightarrow n$ process are known for $n = 2$ and only for some $2 \rightarrow 3$ processes. Among the latter it is worth mentioning the QCD corrections to $pp \rightarrow ZZZ$, WWZ , HHH [8], $pp \rightarrow Hjj$ [9] and $pp \rightarrow t\bar{t}j$ [10]. For $2 \rightarrow 4$ processes, only the QCD corrections to the weak boson fusion $pp \rightarrow WWjj$ [11], $WZjj$ [12] and the complete electroweak $\mathcal{O}(\alpha)$ corrections to $e^+e^- \rightarrow 4$ fermions [13] have been calculated with standard diagrammatic approaches, supplemented with new reduction techniques of scalar and tensor integrals [14]. No complete calculation of NLO QCD corrections to $pp \rightarrow 4$ partons exists at present. Only the calculation of six-gluon scattering amplitudes has been completed successfully [15], even if the needed CPU time renders the calculation unsuited for event generation. Within QED, the calculation of n -photon amplitudes have been performed by several groups, with n up to six [16].

In order to overcome the difficulties in the calculation of virtual corrections to multi-leg processes, several groups have developed new (semi)numerical and analytical techniques. It is worth mentioning the work of Ref. [17], based on the method developed in Ref. [18], which has been used to build up the complete two-loop renormalization program within the Standard Model [?]. Pure numerical algorithms have been proposed in Ref. [20], with applications to e^+e^- annihilations.

The analytical methods exploit the unitarity cut method and on-shell recursion

relations to calculate the so-called cut-constructible part of loop amplitudes (see Ref. [21] for an exhaustive review and references). The method is particularly suited for loop calculations in gauge theories, where the final analytical expressions are quite simple. An efficient algebraic technique, suitable for numerical implementation, has been suggested in Ref. [22]. The main problem of the unitarity cut approach is related to the so-called rational part of the amplitude, for which other methods are required [23]. Very recently, in Ref. [24] it has been proposed an algorithm based on D -dimensional unitarity, which allows the calculation of both cut-constructible and rational parts of one-loop scattering amplitudes. Moreover the method reduces the algorithmic complexity at the polynomial level and it is suited for numerical implementation.

The common feature of the above mentioned techniques is the use of dimensional regularization and the decomposition of the amplitude in linear combinations of basic scalar loop integrals.

In the present note we study an alternative way, of purely numerical nature, for the calculation of loop-amplitudes, exploiting the fact that we have already at hand efficient and well developed numerical tools for the calculation of tree-level scattering amplitudes. We follow the approach suggested by Veltman in Ref. [25], according to which any one-loop amplitude can be written as a convolution of LO amplitudes by means of appropriate dispersion relations. The method has been used in Refs. [25,26] at the formal level to discuss causality for individual diagrams. With a particular way of balancing energy conservation in cut diagrams by adding an ‘artificial particle’, a Feynman graph can be computed by the convolution of LO amplitudes, cutting any two internal lines. The method can be reformulated in terms of amplitudes, rather than in terms of individual Feynman graphs, and in this way we can retain the main advantage of LO approach, namely the power law growth of computational complexity rather than factorial growth.

The numerical nature of the procedure is an added bonus for the automation of the procedure. In the calculation of a scattering cross sections, the loop integration is performed through the Monte Carlo method together with the phase space integration. This leaves two important open problems: the stability of the numerical integration and the regularization method for infrared and collinear singularities, which needs to be performed in four dimensions.

In the following sections we illustrate the method for the simple case of the ϕ^3 model, showing some numerical comparisons between the results obtained with this approach and the standard diagrammatic techniques.

2 Introduction to the method

We shall first shortly review the largest time equation and the dispersion relations “à la Veltman” we shall use in this paper, referring to [25] for further details.¹

For definiteness we work in a ϕ^3 theory, setting the coupling constant to one for simplicity. The propagator for a scalar field, propagating from spacetime point x to y , is

$$\Delta_{xy} = \int \frac{dl}{(2\pi)^4} e^{-il(x-y)} \frac{i}{l^2 - m^2} = \theta(x_0 - y_0) \Delta_{xy}^+ + \theta(y_0 - x_0) \Delta_{yx}^+ \quad (1)$$

$$\Delta_{xy}^+ = \int \frac{dl}{(2\pi)^3} e^{-il(x-y)} \theta(l_0) \delta(l^2 - m^2) \quad (2)$$

For a generic n -point, one-particle irreducible, Feynman diagram G_n we obtain, in configuration space:

$$G_n(x_1, \dots, x_n) = i^n \Delta_{x_1 x_2} \Delta_{x_2 x_3} \dots \Delta_{x_n x_1} \quad (3)$$

where x_j enters clockwise in the diagram (see fig. 1). We now introduce a new notation: the “underlined configuration variable” \underline{x}_j and a new set of functions

$$\begin{aligned} \tilde{G}_n(x_1, \dots, \underline{x}_j, \dots, \underline{x}_k, \dots, x_n) = \\ (-1)^{n_u} i^n \Delta_{x_1 x_2} \dots \Delta_{x_{j-1} \underline{x}_j} \dots \Delta_{x_k \underline{x}_{k+1}} \dots \Delta_{x_n x_1} \end{aligned} \quad (4)$$

where n_u is the number of underlined variables and

$$\begin{aligned} \Delta_{\underline{x}_l x_m} &= \Delta_{x_m x_l}^+ \\ \Delta_{x_l \underline{x}_m} &= \Delta_{x_l x_m}^+ \\ \Delta_{\underline{x}_l \underline{x}_m} &= \Delta_{x_l x_m}^* \end{aligned}$$

Notice that because of the $\theta(l_0)$ term in equation (2) *energy is always required to flow towards the underlined vertex.*

¹ We follow closely ref. [25], using Minkowski metrics and this justify some sign difference and the appearance of constant factors i . We also use the relationship $\Delta_{xy}^+ = \Delta_{yx}^-$ everywhere in the paper.

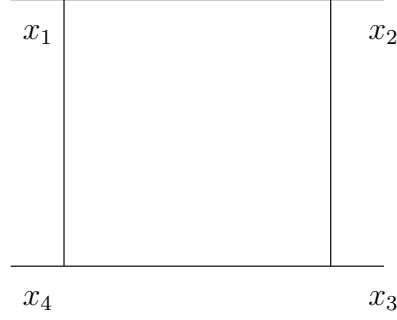


Fig. 1. Four point function $G_4(x_1, x_2, x_3, x_4)$.

We can introduce a diagrammatic notation for the \tilde{G}_n functions: we shall denote with a small circle a vertex to which an underlined variable is “attached”, namely, for example:

$$\tilde{G}(\underline{x}, y, \underline{z}) = \begin{array}{c} x \ominus \quad y \\ \quad \quad \quad \diagdown \quad \diagup \\ \quad \quad \quad z \ominus \end{array}$$

Therefore the set of Feynman rules for an underlined diagram are:

$$\begin{aligned} \text{---} \angle &\equiv i; & \text{---} \ominus &\equiv -i \\ x \text{---} y &\equiv \Delta_{xy}; & x \ominus \text{---} y &\equiv \Delta_{xy}^*; \\ x \text{---} \ominus y &\equiv \Delta_{xy}^+; & x \ominus \text{---} y &\equiv \Delta_{yx}^+ \end{aligned}$$

With the above set of Feynman rules and definitions we obtain

$$x_0 > y_0, z_0 \Rightarrow \tilde{G}(x, y, z) = -\tilde{G}(\underline{x}, y, z); \quad \tilde{G}(x, \underline{y}, z) = -\tilde{G}(\underline{x}, \underline{y}, z); \dots \quad (5)$$

namely if x_0 is the largest time “entering into a given graph” the sum of a \tilde{G} with underlined x and without underlined x is equal to zero. This feature applies to any diagram with an arbitrary number of legs. This observation leads to the largest time equation

$$\sum_{\text{all possible underlings}} \tilde{G}(x_1, \dots, x_n) = 0 \quad (6)$$

which, for the case of a three point function, reads

$$\begin{aligned} &\tilde{G}(x, y, z) + \tilde{G}(\underline{x}, y, z) + \tilde{G}(x, \underline{y}, z) + \tilde{G}(x, y, \underline{z}) + \tilde{G}(\underline{x}, \underline{y}, z) + \tilde{G}(\underline{x}, y, \underline{z}) \\ &+ \tilde{G}(x, \underline{y}, \underline{z}) + \tilde{G}(\underline{x}, y, \underline{z}) = 0 \end{aligned} \quad (7)$$

Indeed if $x_0 > y_0, z_0$ the contributions (1,2), (3,5), (4,6) and (7,8) of Eqn. (7) cancel pairwise. If $y_0 > x_0, z_0$ the cancellation occurs among the (1,3), (2,5), (4,7) and (6,8) pair of diagrams. Finally if $z_0 > x_0, y_0$ the cancellation occurs among the (1,4), (2,6), (3,7) and (4,8) pair of diagrams. This cancellation is explicitly worked out in the appendix. From Eqn. (7) one easily arrive at the standard Cutkowsky rules for the imaginary² part of a diagram

$$\begin{aligned} \tilde{G}(x, y, z) + \tilde{G}(\underline{x}, \underline{y}, \underline{z}) &= G(x, y, z) + G(x, y, z)^* \\ &= - \left[\tilde{G}(\underline{x}, y, z) + \tilde{G}(x, \underline{y}, z) + \tilde{G}(x, y, \underline{z}) + \tilde{G}(\underline{x}, \underline{y}, z) \right. \\ &\quad \left. + \tilde{G}(\underline{x}, y, \underline{z}) + \tilde{G}(x, \underline{y}, \underline{z}) \right] \end{aligned} \quad (8)$$

Since the Feynman rule for a line connecting an ordinary vertex and an underlined one is indeed equivalent to cut the diagram on the corresponding line this is the standard Cutkowsky rule for the imaginary part of the diagram. Notice that several contributions in the above equation vanish, since energy is required to flow from standard to underlined vertices and conflicting conditions might be required to hold simultaneously. By mean of the largest time equation we can derive another equation which allows to formulate a universal dispersive like formula for an arbitrary Feynman graph. We choose any³ two vertices in the diagram of interest, say y and z in the three point function. We have

$$G(x, y, z) = \theta(y_0 - z_0)G(x, y, z) + \theta(z_0 - y_0)G(x, y, z) \quad (9)$$

and

$$\theta(y_0 - z_0) \left[\tilde{G}(x, y, z) + \tilde{G}(x, \underline{y}, z) + \tilde{G}(\underline{x}, y, z) + \tilde{G}(\underline{x}, \underline{y}, z) \right] = 0 \quad (10)$$

Indeed, as discussed in Eqn. (5), if $y_0 > z_0, x_0$ contributions (1,2) and (3,4) cancel pairwise; if $x_0 > y_0, z_0$ contributions (1,3) and (2,4) cancel pairwise; if

² Notice that, using the conventional decomposition of the S matrix $S = I + iT$, $G(x_1, \dots, x_n)$ contributes to iT

³ that's why we choose to discuss both the simpler two point function and the three point one: for the two point function the arbitrariness in the choice of the two vertices has no meaning.

$z_0 > x_0, y_0$ the overall θ function ensures the vanishing of this contribution. From Eqns. (7), (9) and (10) (and the analogous one for the term with $\theta(z_0 - y_0)$) we obtain

$$\begin{aligned}
G(x, y, z) &= -\theta(y_0 - z_0) \left[\tilde{G}(\underline{x}, y, z) + \tilde{G}(x, \underline{y}, z) + \tilde{G}(\underline{x}, \underline{y}, z) \right] \\
&\quad -\theta(z_0 - y_0) \left[\tilde{G}(\underline{x}, y, z) + \tilde{G}(x, y, \underline{z}) + \tilde{G}(\underline{x}, y, \underline{z}) \right] \\
&= -\theta(y_0 - z_0) \left[\tilde{G}(x, \underline{y}, z) + \tilde{G}(\underline{x}, \underline{y}, z) \right] \\
&\quad -\theta(z_0 - y_0) \left[\tilde{G}(x, y, \underline{z}) + \tilde{G}(\underline{x}, y, \underline{z}) \right] - \tilde{G}(\underline{x}, y, z) \tag{11}
\end{aligned}$$

Notice that the last term in Eqn. (11) corresponds to a cut in which the two chosen vertices y and z lie on the same side of the cut. This term is one of the terms occurring in the unitarity relation (8) and is purely real.

For twice the imaginary part of G (real part of the amplitude), from Eqn.(11), we obtain

$$\begin{aligned}
G(x, y, z) - G(x, y, z)^* &= [\theta(y_0 - z_0) - \theta(z_0 - y_0)] \left[\tilde{G}(x, \underline{y}, z) + \tilde{G}(\underline{x}, \underline{y}, z) \right. \\
&\quad \left. - \tilde{G}(x, y, \underline{z}) - \tilde{G}(\underline{x}, y, \underline{z}) \right] \tag{12}
\end{aligned}$$

For the two point function we obtain

$$G(x, y) - G(x, y)^* = [\theta(x_0 - y_0) - \theta(y_0 - x_0)] \left[\tilde{G}(x, \underline{y}) + \tilde{G}(y, \underline{x}) \right] \tag{13}$$

$$G(x, y) + G(x, y)^* = \left[\tilde{G}(x, \underline{y}) + \tilde{G}(y, \underline{x}) \right] \tag{14}$$

This is a dispersion relation for the real part of a generic, one particle irreducible n-point function. In the appendix we verify explicitly that Eqn. (13) holds and we show that inserting the integral representation of the θ function it leads to a dispersive like integral.

We introduce a diagrammatic representation for the θ function appearing in Eqns. (12) and (13): we will connect the two chosen vertices with a wavy line hereafter referred to as the τ -line. Before providing the generic recipe, notice that a function \tilde{G} is non vanishing only if ordinary and underlined vertices belong to two distinct connected regions: the one containing underlined variables will be referred to as shadowed the other one as unshadowed. The energy along the cut lines will flow from the unshaded to the shaded region. We refer to [25] for a thorough discussion and we just give an example of a vanishing contribution to a box function in fig. 2.

For a generic Green function the method can be applied as well and, summarizing the results sketched above, leads to the following modified Feynman

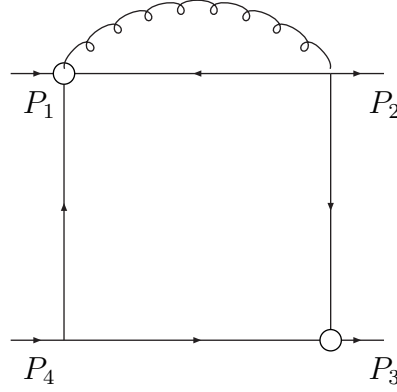


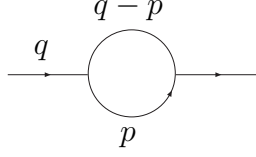
Fig. 2. Vanishing contribution to the four point function. The diagram is split into four disconnected regions (each propagator connecting a dotted and an undotted vertex is on shell). Arrows denote the direction of the energy flow

rules:

- Draw a τ -line (the θ function insertion in Eqn. (9)) between two arbitrary vertices of the Feynman graph.
- Cut the graph in two disconnected parts in such a way that the τ -line crosses (if both the chosen vertices are on the same side of the cut this will contribute only to the imaginary part of the graph as $\tilde{G}(\underline{x}, y, z)$ in Eqn.(11)) the cut.
- In the vertices where the τ -line is absorbed/emitted it does contribute (this and the following items are explicitly shown, for the two point function, in the appendix) to the energy balance with a τ .
- The τ -line contributes a factor $1/(i\pi) \times \oint d\tau (1/\tau)$ (\oint denotes the principal value integral).
- Cut internal lines contribute a factor $\theta(\pm k^0) \delta(k^2 - m^2)$ where $\pm k^0$ is chosen in such a way that their energy flows towards the shaded region.
- A two-body phase space integral is associated with the two cut internal lines: $d\Phi = \lambda^{1/2}(P^2, p_1^2, p_2^2)/P^2 d\cos\theta d\phi$ where $p_{1,2}$ are the momenta of the cut internal lines, and P is the sum of the external 4-momenta k_j which enter into the unshaded part of the graph plus the τ -line contribution which amounts to subtract τ to the time-like P component.
- Sum over the contributions of all allowed cuts (see the items above).

2.1 The two point function

In order to illustrate the method let us start by computing the simplest 1-loop diagram in a scalar ϕ^3 theory (q is off-shell):



Using the standard techniques and omitting all constant factors for the sake of simplicity, this loop diagram is proportional to:

$$\int d^4p \frac{1}{(p^2 - m^2 + i\epsilon)((q - p)^2 + i\epsilon)} = \int_0^1 dx \int d^4p \frac{1}{(p^2 + L(x))^2} \quad (15)$$

where one of the fields in the loop is assumed to be massless and

$$L(x) = x(1 - x)q^2 - (1 - x)m^2. \quad (16)$$

Upon rotation to euclidean momenta and setting an ultraviolet cut-off Λ , the loop integral in (15) reduces to

$$\begin{aligned} & \pi^2 i \int_0^1 dx \int_0^{\Lambda^2} dz \frac{z}{(z - L(x))^2} \simeq \\ & \simeq \pi^2 i \int_0^1 dx [\ln \Lambda^2 - \ln(-x(1 - x)q^2 + (1 - x)m^2)] = \\ & = \pi^2 i \left(\ln \Lambda^2 - \frac{q^2 - m^2}{q^2} \ln |q^2 - m^2| - \frac{m^2}{q^2} \ln m^2 + 2 \right. \\ & \quad \left. + i\pi \frac{q^2 - m^2}{q^2} \theta(q^2 - m^2) \right) \end{aligned}$$

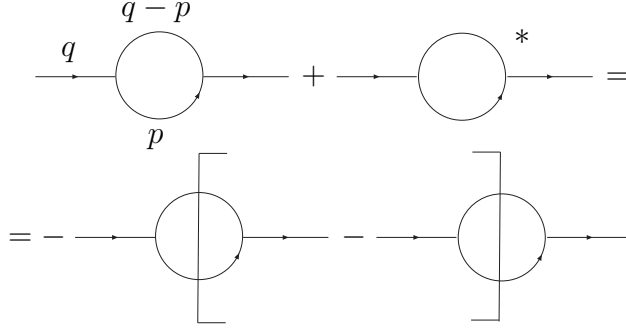
where in the latter step we have used integration by parts, and we have also used $\Lambda^2 \gg q^2, m^2$.

The largest time equation (14), for the two poin function, reads

$$\begin{aligned} G(x, y) + G(x, y)^* &= (\Delta_{xy}^+)^2 + (\Delta_{yx}^+)^2 \\ G(q) + G(q)^* &= -2\pi^3 \frac{q^2 - m^2}{q^2} \theta(q^2 - m^2) \end{aligned}$$

$G(q)$ denoting the fourier transform of $G(x, y)$.

In fact, we have:



where the parenthesis '[' indicates that the shadowed part of the diagram is on the right and vice-versa for ']'. The rule for internal lines flowing towards the shaded region is to associate to them a $\theta(k^0)\delta(k^2 - m)$. For a line flowing out of the shaded region one associates a $\theta(-k^0)\delta(k^2 - m)$. As a result, the latter diagrammatic equation reduces to (apart from an overall sign)

$$\int d^4p [\theta(-q^0 + p^0)\delta((q - p)^2)\theta(p^0)\delta(p^2 - m^2) + \theta(q^0 - p^0)\delta((q - p)^2)\theta(-p^0)\delta(p^2 - m^2)] \quad (17)$$

The first term of the latter expression can be written introducing a Dirac- δ as

$$\int d^4p \int d^4Q \delta^4(q - p - Q)\theta(Q^0)\delta(Q^2)\theta(p^0)\delta(p^2 - m^2). \quad (18)$$

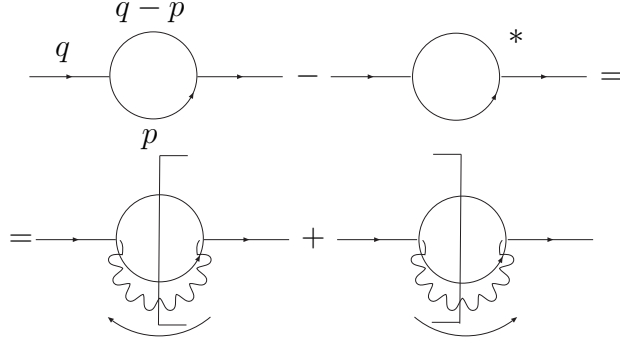
which simply reduces to the phase space factor:

$$\int \frac{d^3p}{2p^0} \frac{d^3Q}{2Q^0} \delta^4(q - p - Q) = \frac{\pi}{2} \frac{\lambda^{1/2}(q^2, m^2, 0)}{q^2} = \frac{\pi}{2} \frac{q^2 - m^2}{q^2} \theta(q^2 - m^2), \quad (19)$$

where the θ factor is the threshold condition $q^2 > m^2$. For simplicity, we have neglected constant factors. Computing also the second integral and accounting for the proper factors of π , one finds (see eq. (17)):

$$F + F^* = -2\pi^3 \frac{q^2 - m^2}{q^2} \theta(q^2 - m^2) \quad (20)$$

Let us now turn to the remaining part of our loop diagram, namely the one obtainable by subtracting $F - F^*$. For this purpose, following [25] we consider the diagrammatic equation:



Here we have a new symbol, the so called τ -line represented by a $\sim\sim\sim\sim\sim$. The τ -line makes energy flow from the unshaded to the shaded areas ⁴. Namely the 4-momentum associated to a τ -line is $\tau^\mu = (\tau, 0, 0, 0)$. Following the prescriptions obtained in [25], the cut τ -line introduces a factor $1/i\pi \times 1/\tau$ and a principal value integral is required. Then the latter diagrammatic equation writes to (apart from overall constant factors):

$$\frac{1}{i\pi} \oint \frac{d\tau}{\tau} \left\{ \frac{\pi}{2} \frac{(q-\tau)^2 - m^2}{(q-\tau)^2} \theta((q-\tau)^2 - m^2) + \frac{\pi}{2} \frac{(q+\tau)^2 - m^2}{(q+\tau)^2} \theta((q+\tau)^2 - m^2) \right\}. \quad (21)$$

Let us make the shifts $q^0 - \tau = -\tau' \rightarrow \tau$ in the first integral and $q^0 + \tau = \tau' \rightarrow \tau$ in the second to obtain

$$\oint d\tau \left\{ \frac{1}{q^0 + \tau} \frac{\tau^2 - \mathbf{q}^2 - m^2}{\tau^2 - \mathbf{q}^2} \theta(\tau^2 - \mathbf{q}^2 - m^2) + \frac{1}{\tau - q^0} \frac{\tau^2 - \mathbf{q}^2 - m^2}{\tau^2 - \mathbf{q}^2} \theta(\tau^2 - \mathbf{q}^2 - m^2) \right\}. \quad (22)$$

Apart from the $1/\tau$ factor, the cut diagrams are invariant and may be evaluated in any frame: we go to the frame $\mathbf{q} = \mathbf{0}$, where the integral in (22)

⁴ More precisely the τ -line ensures: 1) that the energy is conserved on both sides of the cut and 2) that the cut lines *exit* from the unshaded area and *enter* into the shaded one. Therefore the τ -line accounts for an arbitrary amount of energy entering (most likely) the unshaded area and exiting from the shaded one, as indicated by the arrows in the figure.

reduces to

$$\oint d\tau \left\{ \frac{2\tau}{\tau^2 - q^2} \frac{\tau^2 - m^2}{\tau^2} \theta(\tau^2 - m^2) \right\}. \quad (23)$$

Setting $\tau' = -\tau$ and $\tau'^2 = \lambda$ we find

$$\int_{m^2}^{\Lambda^2} d\lambda \frac{\lambda - m^2}{\lambda} \frac{1}{\lambda - q^2}. \quad (24)$$

Solving this integral and using the fact that $\Lambda^2 \gg q^2$ we find:

$$F - F^* = \ln \Lambda^2 - \frac{q^2 - m^2}{q^2} \ln(m^2 - q^2) - \frac{m^2}{q^2} \ln m^2. \quad (25)$$

With the proper constants taken into account we reconstruct the result obtained initially⁵. Indeed from our initial calculation we get:

$$F - F^* = 2\pi^2 i \left(\ln \Lambda^2 - \frac{q^2 - m^2}{q^2} \ln(m^2 - q^2) - \frac{m^2}{q^2} \ln m^2 \right). \quad (26)$$

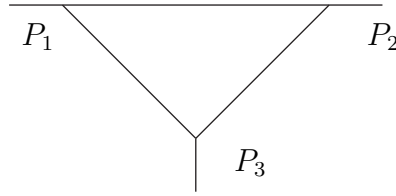


Fig. 3. Three point Green function in a scalar ϕ^3 theory

2.2 The three point function

We consider now a three point scalar function in ϕ^3 theory. The Green function depicted in Fig. 3 is, up to constant factors,

$$G_3(P_1, P_2, P_3) \sim \int d^4 L \frac{1}{[(L - P_1)^2 - m^2][(L - P_1 - P_2)^2 - m^2][L^2 - m^2]},$$

⁵ Actually the two results differ by a constant factor. This is a consequence of the fact that the chosen Green function is divergent and the choice of two different UV regulators leads to a constant shift in the lagrangian parameters.

where $P_j \equiv (\Pi_j, \mathbf{p}_j)$ denotes external momenta, all momenta are assumed incoming, m is the mass of the scalar particle and $L \equiv (L_0, \mathbf{l})$ is the loop four momentum and the standard $L_0 \rightarrow L_0 + i\epsilon$ prescription is understood.

Using the rules explained above we can write:

$$\begin{aligned}
G_3(P_1, P_2, P_3) &\sim A_1 + A_2 + A_3 + A_4, \\
A_1 &\sim \int \frac{d\tau}{\tau + i\epsilon} \int d\mathbf{k}_1 d\mathbf{k}_2 \delta(\Pi_1 - \tau - E_1 - E_2) \\
&\quad \delta(\mathbf{p}_1 - \mathbf{k}_1 - \mathbf{k}_2) \frac{1}{E_1 E_2} \frac{1}{[(K_1 + P_3)^2 - m^2]}, \\
A_2 &\sim \int \frac{d\tau}{\tau + i\epsilon} \int d\mathbf{k}_1 d\mathbf{k}_2 \delta(\Pi_2 + \Pi_3 - \tau - E_1 - E_2) \\
&\quad \delta(\mathbf{p}_2 + \mathbf{p}_3 - \mathbf{k}_1 - \mathbf{k}_2) \frac{1}{E_1 E_2} \frac{1}{[(K_1 - P_3)^2 - m^2]}, \\
A_3 &\sim \int \frac{d\tau}{\tau + i\epsilon} \int d\mathbf{k}_1 d\mathbf{k}_2 \delta(\Pi_1 + \Pi_3 - \tau - E_1 - E_2) \\
&\quad \delta(\mathbf{p}_1 + \mathbf{p}_3 - \mathbf{k}_1 - \mathbf{k}_2) \frac{1}{E_1 E_2} \frac{1}{[(K_1 - P_3)^2 - m^2]}, \\
A_4 &\sim \int \frac{d\tau}{\tau + i\epsilon} \int d\mathbf{k}_1 d\mathbf{k}_2 \delta(\Pi_2 - \tau - E_1 - E_2) \\
&\quad \delta(\mathbf{p}_2 - \mathbf{k}_1 - \mathbf{k}_2) \frac{1}{E_1 E_2} \frac{1}{[(K_1 + P_3)^2 - m^2]},
\end{aligned}$$

where $K_j \equiv (E_j, \mathbf{k}_j) = (\sqrt{|\mathbf{k}_j|^2 + m^2}, \mathbf{k}_j)$

We can draw a τ -line between P_1 and P_2 vertices. We then cut (put on mass-shell) the corresponding internal lines and one of the other internal lines (this gives rise to two contributions corresponding to E_j both positive or negative). We sum over all possible cuts and convolute with the given weight as shown in Fig. 4.

Notice that we have obtained a dispersive formula: each term is the convolution of two tree level Feynman diagrams (with on-shell external particles and with a peculiar vertex where energy conservation is guaranteed only by including the τ -line contribution) times two body phase space times $1/\tau d\tau$ integration very much like the dispersive integral of the imaginary part of an amplitude. This particular dispersive formulation is independent from the specific diagram.

We can go one step further. Let us focus on the contribution A_1 : it is the convolution of the process

$$\phi_1 \rightarrow \phi_1^{(cut)} \phi_2^{(cut)}$$

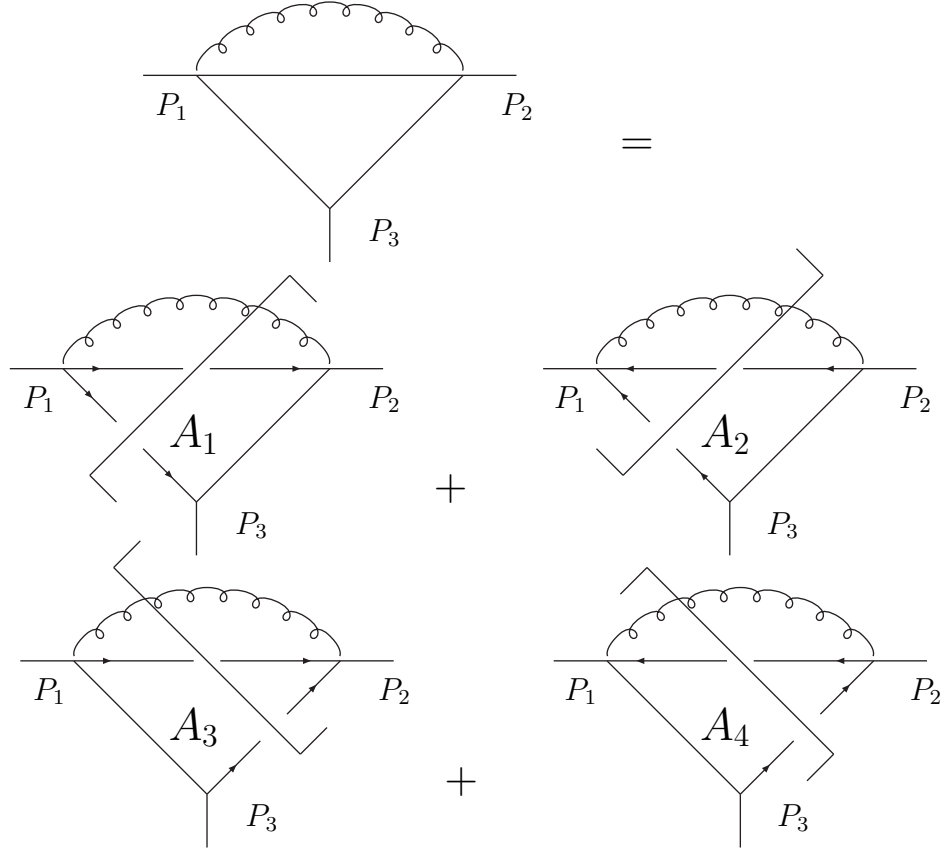


Fig. 4. Three point Green function in a scalar ϕ^3 theory. wavy-line denotes the dispersive integral over $d\tau$ as well as internal two body phase space. The arrows on internal cut lines depict the energy flow in the cut diagram.

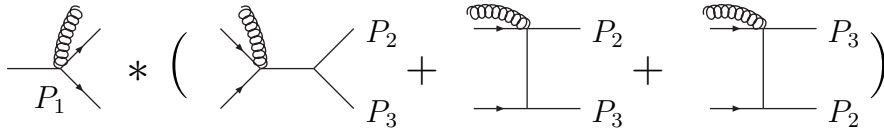


Fig. 5. Convolution of amplitudes rather than individual Feynman graphs. It is manifest that, in addition to vertex contributions, we pick up also self energies contributions.

and the t -channel graph for the process

$$\phi_1^{(cut)} \phi_2^{(cut)} \rightarrow \phi_2 \phi_3, \quad (27)$$

where ϕ_j denotes external particles with momentum P_j and $\phi_j^{(cut)}$ denotes internal (cut) particles. If we extend A_1 to include the contribution of the whole amplitude (s , t , and u channel contributions, see Fig. 5) of process (27), we also obtain the contribution of the ϕ_1 external self-energies as well as part of the triangles for the process

$$\phi_1 \rightarrow \phi_2 \phi_3. \quad (28)$$

Applying the same procedure to all the A_j graphs, we obtain the one-loop correction to the amplitude for the process (28) as given by the formula

$$\begin{aligned} \phi_1 \rightarrow \phi_2 \phi_3 \equiv & \sum_{\substack{j_1, j_2, j_3=1,3 \\ j_1 \neq j_2, j_1 \neq j_3, j_2 \neq j_3}} (\phi_{j_1} \phi_{j_2} \rightarrow \phi_1^{(cut)} \phi_2^{(cut)}) * (\phi_1^{(cut)} \phi_2^{(cut)} \rightarrow \phi_{j_3}) \\ & + (\phi_{j_1} \rightarrow \phi_1^{(cut)} \phi_2^{(cut)}) * (\phi_1^{(cut)} \phi_2^{(cut)} \rightarrow \phi_{j_2} \phi_{j_3}), \end{aligned}$$

where with the symbol $*$ we denote the convolution with the two body phase space and the dispersive integral over $d\tau$. Actually, to define unambiguously the above expression one needs a prescription to pick up the two vertices where energy conservation is ensured by the τ -line contribution, and one needs to check that each diagram is accounted for with the correct combinatorial factors. This will be discussed later on.

We have thus achieved our first goal: with the algorithm sketched above we can write any one loop amplitude as a convolution in 4-dimensions of tree level amplitudes. More precisely, given a set of external particles, we divide it into two non empty subsets \mathcal{G}_{α_j} $j = 1, 2$. We compute the convolution of

$$(\mathcal{G}_{\alpha_1} \rightarrow \chi_1 \chi_2) * (\chi_1 \chi_2 \rightarrow \mathcal{G}_{\alpha_2}), \quad (29)$$

summing over all possible intermediate particles χ_j (here “possible” means compatible with the symmetries of the theory). Recall that tree-level amplitudes are computed for on-shell particles but an arbitrary amount of energy can outflow/sink from/in one vertex. Therefore one of the two amplitudes in (29) can be non zero also for all particles incoming/outgoing. Finally we sum over all possible \mathcal{G}_{α_1} , \mathcal{G}_{α_2} partitions.

3 The general algorithm

In this section we outline the general algorithm we use to draw the τ -lines and to select all the cut diagrams with the proper weights and combinatorial factors.

For definiteness we consider the amplitude

$$\phi(P_1)\phi(P_2) \rightarrow \phi(P_3)\phi(P_4) \quad (30)$$

in ϕ^3 theory. P_j denote, as before, the momenta of the external particles.

- We divide the set of external particles into two non empty subsets \mathcal{G}_{α_j} $j = 1, 2$. There are 14 $\left(= \sum_{i=1}^3 \binom{4}{i} \right)$ such partitions.
- We compute the convolution of

$$[\mathcal{G}_{\alpha_1} \rightarrow \phi(K_1)\phi(K_2)] * [\phi(K_1)\phi(K_2) \rightarrow \mathcal{G}_{\alpha_2}] \quad (31)$$

summing over all possible partitions. We have denoted with K_j the momenta of the cut lines.

- Require that the τ line is emitted/absorbed at the opposite ends of the cut-line carrying K_1 momentum.
- Select an external momentum (arbitrarily). For definiteness we choose P_1 . We will call it reference momentum from here on.
- If the reference momentum belongs to \mathcal{G}_{α_2} the amplitude for $\mathcal{M}_2 = \phi(K_1)\phi(K_2) \rightarrow \mathcal{G}_{\alpha_2}$ needs to be modified as follows:
 - If a diagram has a propagator depending on a momentum $Q = \sum_j Q_j$, where $Q_j \neq K_1$ and at least P_1 and K_2 enter the sum over j , this diagram must be vetoed.
 - If a diagram has a propagator containing K_1 and at least an external P_j but not P_1 , this diagram must be vetoed.
 - The diagram of \mathcal{M}_2 with K_1 and K_2 attached to the same vertex should be vetoed if \mathcal{G}_{α_1} is made up of a single external particle. This prescription allows us to avoid to compute external particle self energies. This contributions will be computed analytically and added in a second step.
- The above prescriptions will apply also to $\mathcal{G}_{\alpha_1} \rightarrow \phi(K_1)\phi(K_2)$ if P_1 belongs to \mathcal{G}_{α_1} .

Let us examine one of such partitions:

$$\mathcal{G}_{\alpha_1} = \{\phi(P_4)\}; \quad \mathcal{G}_{\alpha_2} = \{\phi(P_1), \phi(P_2), \phi(P_3)\}$$

The calculation of the convolution $\mathcal{M}_{\alpha_1} * \mathcal{M}_{\alpha_2}$ for such partition is sketched in Fig. 10. Vetoed Feynman diagrams are marked in the figure. Summing up over all fourteen partitions one can check by inspection that all contributions to NLO correction are correctly taken into account and that any relevant cut occurs the correct number of times.

After providing the recipe, let us try to motivate it. We shall discuss one of the box diagrams contributing to the amplitude in Eqn. (30). As shown in fig. 6

there are six possible different ways to draw the τ -line, four corresponding to the τ -line emitted and absorbed by two nearby vertices and two corresponding to the τ -line emitted and absorbed by two opposite vertices.

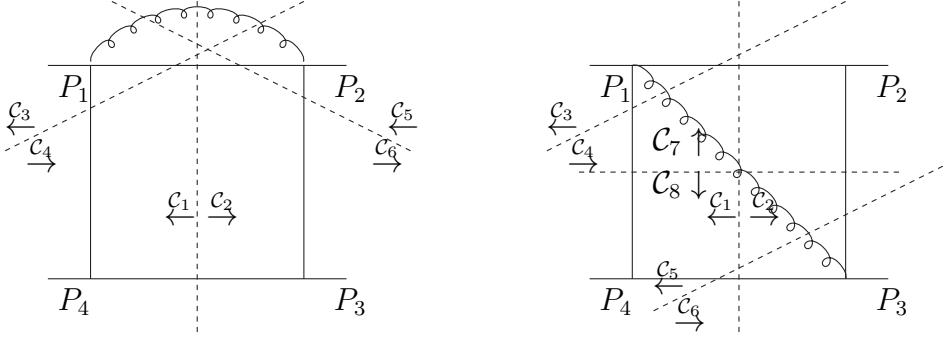


Fig. 6. Four point function. There are six possible ways to draw the τ -line: four as shown in the left-hand side of the figure (the other three possibilities are similar but with the τ -line among P_2 and P_3 or P_3 and P_4 or P_4 and P_1) and two as shown in the right-hand side of the figure (the other one is similar but with the τ -line among P_2 and P_4). The left hand choice gives the sum of six contributions corresponding to having the propagator connecting P_1 and P_2 cut together with anyone of the remaining propagators. The right hand choice gives eight contributions corresponding to having a cut propagator between P_1 and P_2 or between P_2 and P_3 , together with the propagator between P_3 and P_4 or between P_4 and P_1 . Recall that each “cut” actually corresponds to two contributions depending on the energy flow.

Let us focus on the case of the τ -line between two near-by vertices: ⁶ the diagrams will be written as the sum over six possible cuts. If we denote by π_{ij} the propagator connecting P_i and P_j and by (π_{jk}, π_{lm}) the contribution corresponding to π_{jk} and π_{lm} cut propagators, the left-hand diagram of fig. 6 will result from the sum of the (π_{12}, π_{41}) , (π_{12}, π_{34}) and (π_{12}, π_{23}) cuts, each counting as two distinct cuts depending on the energy flow. Each of these contributions will be included into a different term of the convolution of Eqn. (31), namely it will arise with a different choice of α_j (notice that on the opposite sides of the cuts in Fig. 6 there are different sets of external particles). Therefore we need a prescription to ensure that all the cuts enter into the final sum with the same combinatorial factor and that we do not have contributions from the other possible ways of drawing the τ -line.

The simplest prescription is to require that the τ -line is emitted and absorbed together with particle $\phi(K_1)$, namely it will enter/exit always from the vertices

⁶ The other choice is possible as well. It requires a somewhat more involved algorithm. We have not studied it insofar since at present we do not have a good reason to believe it leads to easier integrals.

to which $\phi(K_1)$ is attached. In this way the τ -line is always emitted and reabsorbed at the opposite side of *one* propagator and we single out the topology we are after (left panel of Fig. 6).

If we allow $\phi(K_1)$ to connect to all possible external particles, the diagram of Fig. 6 (left panel) would be reconstructed four times, since the τ -line would connect all possible near-by vertices. With the same reasoning it's easy to conclude that a n -point diagram will be recovered n times.

To adjust the combinatorial factors, we introduce the reference momentum P_1 : we require that $\phi(K_1)$ is attached to the same vertex with $\phi(P_1)$ or with a tree of external particles containing $\phi(P_1)$ as shown in fig. 7. Notice that in this way we obtain each diagram twice (the $\phi(K_1)$ vertex has *two* near-by vertices) with the exception of self-energy contributions which are generated only once. These are indeed the correct combinatorial factors.

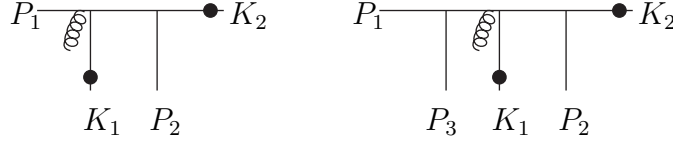


Fig. 7. Allowed particles tree into the amplitudes entering into the convolution of Eqn. (31). Cut propagators (denoted with a small circle) carry momentum K_j and external particles carry momentum P_j . The τ -line is always emitted/absorbed from a vertex connected either directly to P_1 (left-hand side) or to a tree made up of external particles only (K_2 not allowed) and containing P_1 . Equivalently, if the tree is seen from the opposite side, the τ -line is always emitted/absorbed from a vertex connected to a tree made up of external particles plus K_2 and not containing P_1 . The left-hand side diagram, inside the convolution, will contribute to the evaluation of boxes and triangles, whereas the right-hand side to triangles only.

All the prescriptions given above to veto certain contributions to the amplitudes aim at implementing the above reasoning. They amount to require that any particle tree starting from $\phi(P_1)$, to be accepted, should absorb $\phi(K_1)$ *before* $\phi(K_2)$, as shown in Figs. (7) and (8). They look somewhat involved since, due to four-momentum conservation, the momentum flowing into a given propagator can be computed via two possible combinations of particles and we do not know a priori which will be chosen from our tool for the automatic evaluation of tree-level amplitudes. Therefore we cannot simply check if K_1 and P_1

enter into the "same" (in the extended sense described above) vertex, but we need also to check (and accept) also trees made up of external particles $\phi(P_j)$ ($j \neq 1$) and/or $\phi(K_2)$

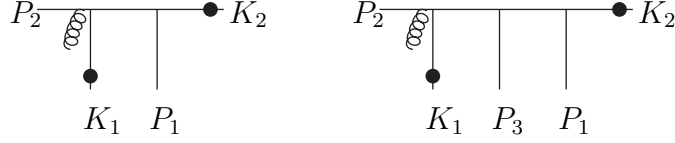


Fig. 8. Vetoed particles tree into the amplitudes entering into the convolution of Eqn. (31). Cut propagators (denoted with a small circle) carry momentum K_j and external particles carry momentum P_j . The K_2 particle is always emitted/absorbed from a vertex connected either directly to P_1 (left-hand side) or to a tree made up of external particle only (K_1 not allowed) and containing P_1 . Equivalently, if the tree is seen from the opposite side, the K_1 particle is always emitted/absorbed from a vertex connected to a tree, made up of external particles, which does not contain neither K_2 nor P_1 .

Coming back to the four point function we sketch in fig. 9 the way it arises from the convolution in Eqn. (31). For simplicity we limit to a single box contributing to the amplitude and denote with dots all the remaining contributions. As shown in fig. 9 the box is evaluated twice corresponding to two different ways of drawing the τ -line.

The various cuts, denoted with \mathcal{C}_j in fig. 9, arise as follows in Eqn. (31)

$$\begin{aligned}
[\mathcal{G}_1 \rightarrow \phi(K_1)\phi(K_2)] * [\phi(K_1)\phi(K_2) \rightarrow \mathcal{G}_{2,3,4}] &= \mathcal{C}_2 + \mathcal{C}_8 + \dots \\
[\mathcal{G}_2 \rightarrow \phi(K_1)\phi(K_2)] * [\phi(K_1)\phi(K_2) \rightarrow \mathcal{G}_{1,3,4}] &= \mathcal{C}_6 + \dots \\
[\mathcal{G}_3 \rightarrow \phi(K_1)\phi(K_2)] * [\phi(K_1)\phi(K_2) \rightarrow \mathcal{G}_{1,2,4}] &= \dots \\
[\mathcal{G}_4 \rightarrow \phi(K_1)\phi(K_2)] * [\phi(K_1)\phi(K_2) \rightarrow \mathcal{G}_{1,2,3}] &= \mathcal{C}_{12} + \dots \\
[\mathcal{G}_{1,2} \rightarrow \phi(K_1)\phi(K_2)] * [\phi(K_1)\phi(K_2) \rightarrow \mathcal{G}_{3,4}] &= \mathcal{C}_{10} + \dots \\
[\mathcal{G}_{1,3} \rightarrow \phi(K_1)\phi(K_2)] * [\phi(K_1)\phi(K_2) \rightarrow \mathcal{G}_{2,4}] &= \dots \\
[\mathcal{G}_{1,4} \rightarrow \phi(K_1)\phi(K_2)] * [\phi(K_1)\phi(K_2) \rightarrow \mathcal{G}_{2,3}] &= \mathcal{C}_4 + \dots \\
[\mathcal{G}_{2,3} \rightarrow \phi(K_1)\phi(K_2)] * [\phi(K_1)\phi(K_2) \rightarrow \mathcal{G}_{1,4}] &= \mathcal{C}_3 + \dots \\
[\mathcal{G}_{2,4} \rightarrow \phi(K_1)\phi(K_2)] * [\phi(K_1)\phi(K_2) \rightarrow \mathcal{G}_{1,3}] &= \dots \\
[\mathcal{G}_{3,4} \rightarrow \phi(K_1)\phi(K_2)] * [\phi(K_1)\phi(K_2) \rightarrow \mathcal{G}_{1,2}] &= \mathcal{C}_9 + \dots \\
[\mathcal{G}_{1,2,3} \rightarrow \phi(K_1)\phi(K_2)] * [\phi(K_1)\phi(K_2) \rightarrow \mathcal{G}_4] &= \mathcal{C}_{11} + \dots \\
[\mathcal{G}_{1,2,4} \rightarrow \phi(K_1)\phi(K_2)] * [\phi(K_1)\phi(K_2) \rightarrow \mathcal{G}_3] &= \dots \\
[\mathcal{G}_{1,3,4} \rightarrow \phi(K_1)\phi(K_2)] * [\phi(K_1)\phi(K_2) \rightarrow \mathcal{G}_2] &= \mathcal{C}_5 + \dots \\
[\mathcal{G}_{2,3,4} \rightarrow \phi(K_1)\phi(K_2)] * [\phi(K_1)\phi(K_2) \rightarrow \mathcal{G}_1] &= \mathcal{C}_1 + \mathcal{C}_7 \dots
\end{aligned}$$

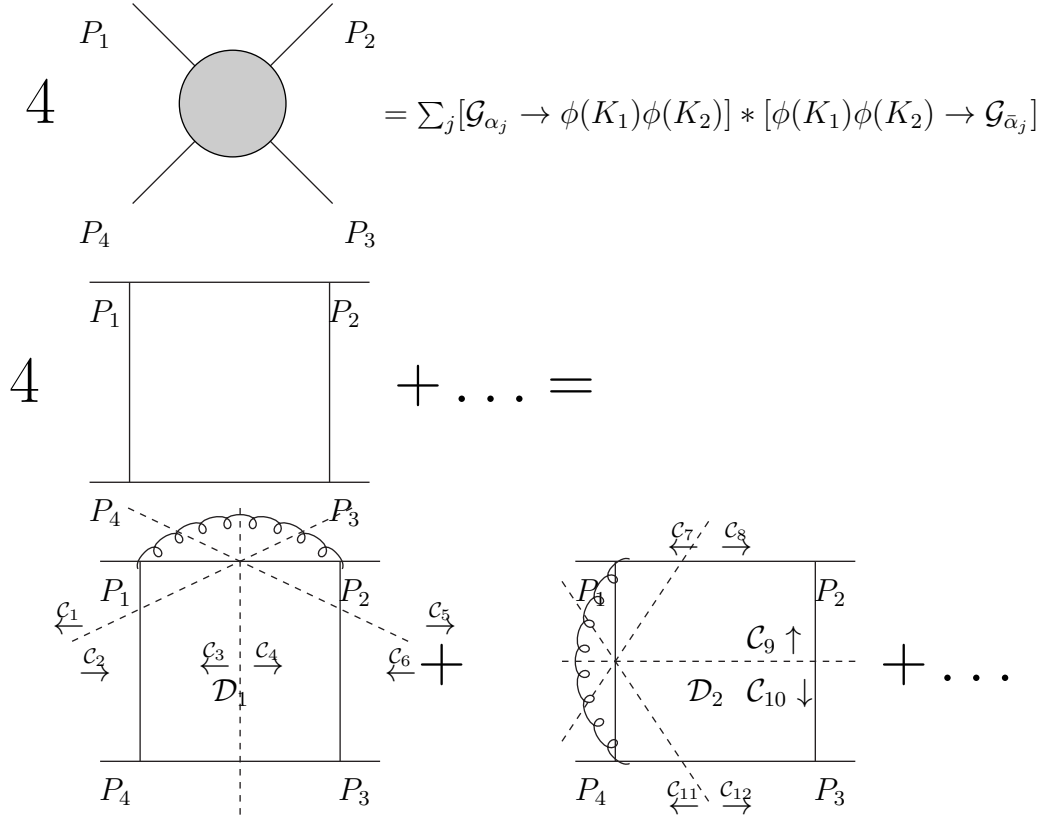


Fig. 9. Cuts contributing to the four point function. Only those relevant to a specific box are shown

The above algorithm applies also to more complex cases with one important addition:

- If cut particles are not identical, one needs to consider both the contribution with $K_1 \leftrightarrow K_2$. Namely the contribution of τ -line absorbed/emitted from K_1 with the above vetoing prescriptions plus the contribution of τ -line absorbed/emitted from K_2 with the above vetoing prescriptions but with $K_1 \leftrightarrow K_2$. The sum of this two contributions leads to twice the results and again one can check by direct inspection that the combinatorics of cut diagrams is correct.

The entire procedure is numerical: we perform a numerical integration *simultaneously* over the *phase space variables of external particles*, over $d\tau$ and *phase space variables of intermediate particles*. Each computation is performed in four space-time dimensions. If needed the integral in $d\tau$ is truncated at $\tau < \tau_{\max}$ (where τ_{\max} is an ultraviolet cutoff) and proper counterterms are included to ensure that the integral is properly regularized. In practice one computes a subtracted Green function and then modifies the tree-level Lagrangian with appropriate counterterms in such a way to reproduce the correct results

for divergent Green functions.

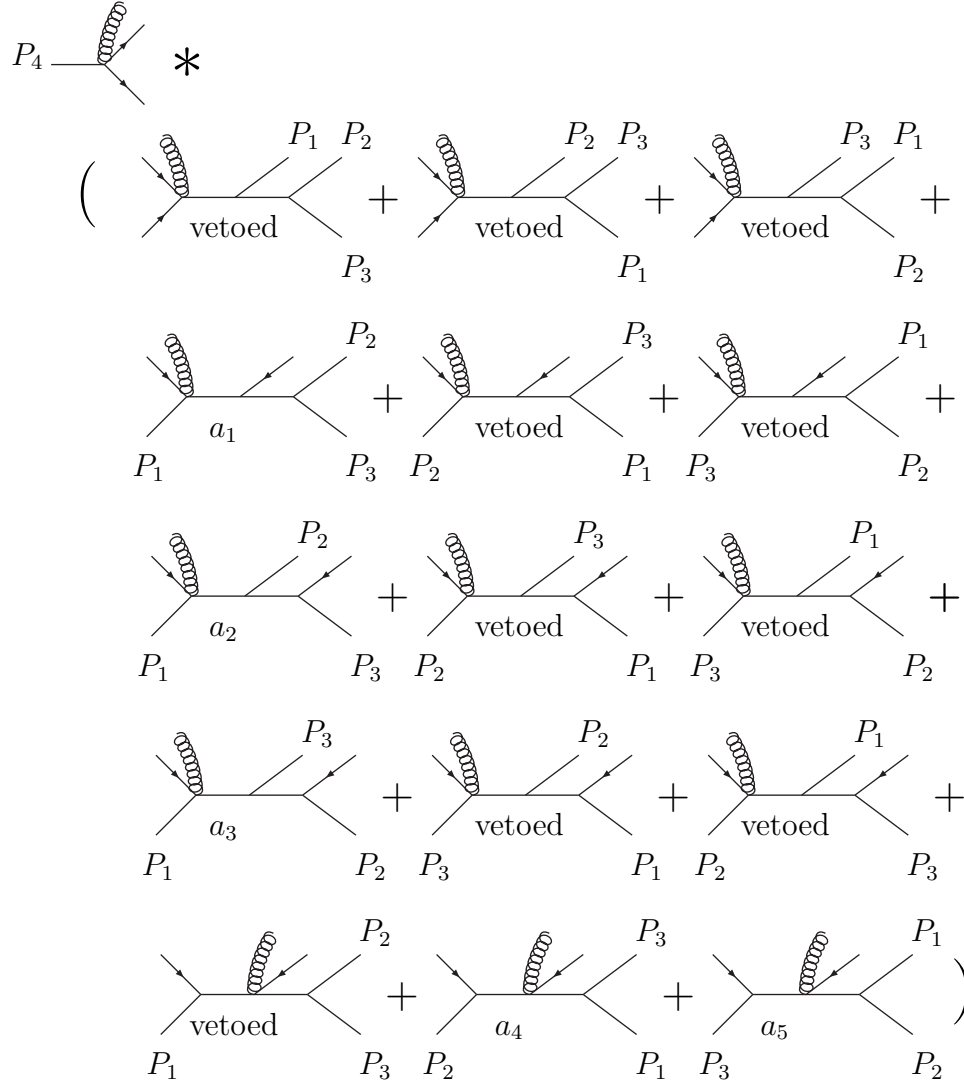


Fig. 10. Convolution of amplitudes rather than individual Feynman graphs. Cut lines carry an arrow. τ -line indicates a τ -line. The graphs contained in the picture correspond to one of the fourteen partitions of the external momenta. The non-vetoed graphs correspond to different one-loop diagrams: a_1 , a_4 and a_5 are cuts contributing to three different triangles, whereas a_2 and a_3 contribute to two different box diagrams. Considering the whole set of fourteen partitions, one recovers the full four-point Green function.

4 Numerical results

We give, in this section, few examples of results obtained with the above described numerical method compared to standard analytic evaluation of loop integrals [28]. More complete numerical results will be shown elsewhere. First of all we give the predictions in Tabs. 1, 2, 3 for the three-, four- and five-points scalar form factors respectively, defined in Eq. 32, in the ϕ^3 scalar theory. We compare only the real part of the form factors, since the method illustrated in the previous sections allows to calculate it. The imaginary part can be easily calculated with standard Cutkowsky rules. This is much easier than the real part, since the required integration over the internal cut lines is only the 2-body phase-space and no dispersion integral is required. Moreover, no principal value integration is needed⁷.

$$\begin{aligned} C_0 &= \frac{1}{i\pi^2} \int d^4q \frac{1}{d_1 d_2 d_3}, \\ D_0 &= \frac{1}{i\pi^2} \int d^4q \frac{1}{d_1 d_2 d_3 d_4}, \\ E_0 &= \frac{1}{i\pi^2} \int d^4q \frac{1}{d_1 d_2 d_3 d_4 d_5}, \end{aligned} \tag{32}$$

where

$$d_1 = (q^2 - m^2 + i\epsilon)$$

⁷ For the real part of the amplitude we deal with the numerical evaluation of principal value integrals using the following strategy. For simplicity let's assume we have to perform the principal value integral of a function $f(x)$ with a pole in x_0 . We can either perform the integral of

$$f_1(x) = \frac{1}{2}[f(x) + f(2x_0 - x)]$$

or, use integration by part,

$$\begin{aligned} \int f(x) \frac{x - x_0}{x - x_0} dx &\rightarrow \log|x - x_0|(x - x_0)f(x) \\ &\quad - \int \log|x - x_0| \frac{d}{dx}[(x - x_0)f(x)] dx \end{aligned}$$

in both cases obtaining a *numerically* convergent integral. Both methods have been explored and tested. (We however need to study computationally more involved examples to be sure that numerical instabilities do not arise because of nearby poles or soft/collinear enhancements). Notice that we can apply the method here sketched since we can easily evaluate analytically the location of the poles as a function of the integration variables.

	p_x (GeV)	p_y (GeV)	p_z (GeV)
p_1	1.73205081	1.41421354	-2.23606801
p_2	-1.73205081	-1.41421354	2.23606801
p_3	0	0	0
	Re(C_0)	1.982(2) (numerical)	1.98390995 Ref. [29]

Table 1

Comparison between the values of the scalar form factor C_0 for the ϕ^3 theory as obtained with the numerical method and with the analytical results of LoopTools [29]. The momenta components are taken to be $p = (p_x, p_y, p_z)$, with a common internal and external mass of 0.01 GeV.

	p_x (GeV)	p_y (GeV)	p_z (GeV)
p_1	1.73205081	1.41421354	-2.23606801
p_2	-1.73205081	-1.41421354	2.23606801
p_3	-2.23606801	-1.41421354	-1.73205081
p_4	2.23606801	1.41421354	1.73205081
	Re(D_0)	0.4435(2) (numerical)	0.443615191 Ref. [29]

Table 2

Comparison between the values of the scalar form factor D_0 for the ϕ^3 theory as obtained with the numerical method and with the analytical results of LoopTools [29]. The momenta components are taken to be $p = (p_x, p_y, p_z)$, with a common internal and external mass of 0.01 GeV.

	p_x (GeV)	p_y (GeV)	p_z (GeV)
p_1	0	0	2.13816766718398
p_2	0	0	-2.13816766718398
p_3	-0.825139760971069	-0.878521561622620	-0.08667117357254028
p_4	-0.501121819019318	-0.772821187973022	-0.162467777729034
p_5	1.32626157999039	1.65134274959564	0.249138951301575
	Re(E_0)	-10.48(2) (numerical)	-10.4724461 Ref. [29]

Table 3

Comparison between the values of the scalar form factors for the ϕ^3 theory as obtained with the numerical method and with the analytical results of LoopTools [29]. The momenta components are taken to be $p = (p_x, p_y, p_z)$, with a common internal and external mass of 0.01 GeV.

$$d_i = ((q + k_{i-1})^2 - m^2 + i\epsilon)$$

and k_i are related to the external momenta as $p_1 = k_1$, $p_n = k_n - k_{(n-1)}$.

In addition we compare the pure virtual NLO QCD correction to $e^+e^- \rightarrow$

fermion mass (GeV)	analytical (nb)	numerical (nb)
1	-1.0622(2)	-1.0623(3)
2	-0.7879(1)	-0.7882(3)
3	-0.5985(1)	-0.5989(2)
8	+0.01320(0)	+0.01289(8)
9	+0.10271(0)	+0.10258(6)

Table 4

Values of the virtual QCD cross section for the process $e^+e^- \rightarrow \gamma^* \rightarrow q\bar{q}$, at $\sqrt{s} = 20$ GeV, for different fermion masses. The infrared divergence has been regulated with a photon mass $m_\gamma = 30$ MeV.

$q\bar{q}$ production (limited to the photon exchange case), at $\sqrt{s} = 20$ GeV and for different values of the fermion mass. The infrared singularity has been regulated giving a mass of 30 MeV to the gluon. Since no QCD non-abelian vertex is present the gluon mass can be safely used. The QCD coupling g_s has been set to 1 for simplicity.

For $e^+e^- \rightarrow q\bar{q}$ there is a divergent 3-point function. We deal with the renormalization problem as follows:

- We compute the 3-point function using a hard cut-off τ_{\max} .
- For a specific external momenta configuration we compute the 3-point Green function both using the hard cut-off τ_{\max} , obtaining $G_3^{(\tau_{\max})}$, and with a conventional regularization, e.g. dimensional regularization (DR), obtaining $G_3^{(DR)}$.
- We then add to the Lagrangian the counterterm $G_3^{(DR)} - G_3^{(\tau_{\max})} = \bar{\psi}(a_0^{(\tau_{\max})}\gamma_0 A_0 - a^{(\tau_{\max})}\gamma \cdot \mathbf{A})\psi$.

5 Conclusions

We have proposed a new approach to the evaluation of one-loop scattering amplitudes in perturbative quantum field theory. In the present paper we have presented the method via some basic examples of one-loop amplitudes in ϕ_4^3 field theory. The basic rules of our calculation approach have been briefly illustrated.

We have calculated few scalar Green functions and evaluated the QCD next-to-leading order correction to $e^+e^- \rightarrow \gamma^* \rightarrow q\bar{q}$ finding very good agreement with analytical results.

To assess the viability of the approach there are still several steps to be faced.

We plan to:

- Apply the method to the evaluation of n-photon amplitudes in QED.
- Explore the feasibility of a regularization based on a hard momentum cut-off both in the ultraviolet and in the infrared region for non abelian gauge theories. This should be possible provided a suitable number of counterterms is introduced in the Lagrangian [27].
- Reproduce available results in $e^+e^- \rightarrow \text{jets}$ at next-to-leading order accuracy.
- Establish the relationship among our regularization scheme and the standard dimensional regularization in order to be able to use existent parton distribution functions.

Acknowledgments

We are grateful to S. Catani and G. Marchesini for useful discussions.

6 Appendix A

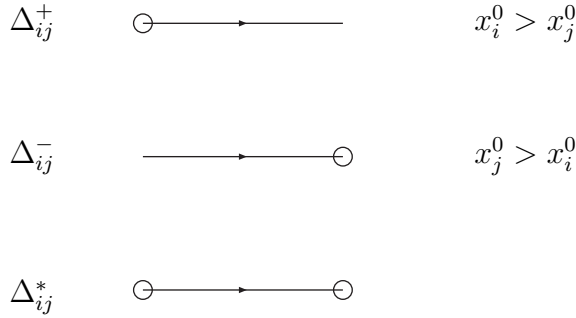


Fig. 11. Feynman rules for propagators involving at least one dotted vertex

For the self energy diagram we have (see Eqn.(1))

$$\begin{aligned}
G(x, y) &= \Delta_{xy} \Delta_{yx} = (\vartheta_{xy} \Delta_{xy}^+ + \vartheta_{yx} \Delta_{yx}^-) (\vartheta_{yx} \Delta_{yx}^+ + \vartheta_{xy} \Delta_{xy}^-) \\
&= \vartheta_{xy} (\Delta_{xy}^+)^2 + \vartheta_{yx} (\Delta_{yx}^+)^2 \\
&= \vartheta_{xy} \left\{ \frac{1}{(2\pi)^6} \int d^4k \, d^4q \exp[-i(x-y)(k+q)] \right. \\
&\quad \left. \times \vartheta(k^0) \vartheta(q^0) \delta(k^2 - m_1^2) \delta(q^2 - m_2^2) \right\} \\
&\quad + \vartheta_{yx} \left\{ \frac{1}{(2\pi)^6} \int d^4k \, d^4q \exp[-i(y-x)(k+q)] \right.
\end{aligned}$$

$$\times \vartheta(k^0)\vartheta(q^0)\delta(k^2 - m_1^2)\delta(q^2 - m_2^2)\}, \quad (33)$$

where $\vartheta_{yx} = \theta(x_0 - y_0)$. We can now introduce an integral representation for the θ function

$$\theta(x) = \frac{1}{2\pi i} \int \frac{e^{i\tau x}}{\tau - i\epsilon} d\tau,$$

with $\epsilon \rightarrow 0^+$ and Eqn. (33) becomes

$$\begin{aligned} G(x, y) &= \frac{1}{2\pi i} \int d\tau \frac{\exp[i\tau(x^0 - y^0)]}{\tau - i\epsilon} \\ &\times \left\{ \frac{1}{(2\pi)^6} \int d^4k d^4q \exp[-i(x - y)(k + q)] \right. \\ &\quad \times \vartheta(k^0)\vartheta(q^0)\delta(k^2 - m_1^2)\delta(q^2 - m_2^2) \Big\} \\ &+ \frac{1}{2\pi i} \int d\tau \frac{\exp[-i\tau(x^0 - y^0)]}{\tau - i\epsilon} \\ &\times \left\{ \frac{1}{(2\pi)^6} \int d^3k d^3q \exp[-i(y - x)(k + q)] \right. \\ &\quad \times \vartheta(k^0)\vartheta(q^0)\delta(k^2 - m_1^2)\delta(q^2 - m_2^2) \Big\} \end{aligned}$$

Since we want to compute the self energy in momentum space, we perform the Fourier transform

$$G(p_1, p_2) = \int e^{ip_1x} e^{ip_2y} G(x, y) dx dy \stackrel{w=x+y}{=} \int e^{ip_1x} e^{ip_2(w+x)} G(w) dx dw$$

and we obtain

$$\begin{aligned} G(p_1, p_2) &= \frac{1}{(2\pi)^3 i} (2\pi)^4 \delta(p_1 + p_2) \\ &\int d\tau \int d^4k d^4q \frac{1}{\tau - i\epsilon} \delta^3(p_2 + k + q) \vartheta(k^0)\vartheta(q^0)\delta(k^2 - m_1^2)\delta(q^2 - m_2^2) \\ &\times [\delta(\tau + p_{20} + k_0 + q_0) + \delta(\tau - p_{20} + k_0 + q_0)] \\ &= \frac{1}{(2\pi)^3 i} (2\pi)^4 \delta(p_1 + p_2) \int d\tau \frac{1}{\tau - i\epsilon} \int d^3k \frac{1}{2k_0} \frac{1}{2q_0} \\ &\times [\delta(\tau + p_{20} + k_0 + q_0) + \delta(\tau - p_{20} + k_0 + q_0)] \end{aligned} \quad (34)$$

where, to perform x and w integrations, we have used $\int e^{ikx} d^4x = (2\pi)^4 \delta^4(k)$

and $k_0 = \sqrt{k^2 + m_1^2}$, $q_0 = \sqrt{(p_2 + k)^2 + m_2^2}$. Recalling that

$$\int \frac{f(\tau)}{\tau - i\epsilon} d\tau = \oint \frac{f(\tau)}{\tau} d\tau + i\pi \int f(\tau) \delta(\tau) d\tau$$

we obtain

$$\begin{aligned} G(p_1, p_2) = & \frac{1}{(2\pi)^{3_i}} (2\pi)^4 \delta(p_1 + p_2) \left\{ \oint d\tau \frac{1}{\tau} \int d^3k \frac{1}{2k_0} \frac{1}{2q_0} \right. \\ & \times [\delta(\tau + p_{20} + k_0 + q_0) + \delta(\tau - p_{20} + k_0 + q_0)] \\ & \left. + i\pi \int d^3k \frac{1}{2k_0} \frac{1}{2q_0} \delta(p_{20} - k_0 - q_0) \right\} \end{aligned} \quad (35)$$

where we assume $p_{20} > 0$ and thus $\delta(p_{20} + k_0 + q_0) = 0$. We can work in the p_2 rest-frame where $k_0 = \sqrt{k^2 + m_1^2}$, $q_0 = \sqrt{k^2 + m_2^2}$. The phase space volume d^3k can be written as $k^2 dk d\Omega$ and the integral over dk can be performed eliminating the δ functions in Eqn. (35) and we finally obtain

$$\begin{aligned} G(p_1, p_2) = & \frac{1}{(2\pi)^{3_i}} (2\pi)^4 \delta(p_1 + p_2) \left\{ \oint_{-\infty}^{-m_1 - m_2 - p_{20}} d\tau \frac{1}{\tau} \int d\Omega \frac{k_+}{-\tau - p_{20}} \right. \\ & \left. + \oint_{-\infty}^{-m_1 - m_2 + p_{20}} d\tau \frac{1}{\tau} \int d\Omega \frac{k_-}{-\tau + p_{20}} + i\pi \int d\Omega \frac{k_i}{p_{20}} \right\} \\ k_{\pm}^2 = & \frac{(p_{20} \pm \tau)^2}{4} - \frac{m_1^2 + m_2^2}{2} + \frac{(m_1^2 - m_2^2)^2}{4(p_{20} \pm \tau)^2} \\ k_i^2 = & \frac{p_0^2}{4} - \frac{m_1^2 + m_2^2}{2} + \frac{(m_1^2 - m_2^2)^2}{4p_{20}^2} \end{aligned}$$

The last term correspond to the real part of the diagram and is indeed equal to half the contribution found, in Eqn. (20), using the largest time equation. The first two terms correspond to the imaginary part of the integrals and coincide with the result of Eqn. (25). Notice that the dispersive integral over $d\tau$ arises as a consequence of using the integral representation for the θ function, thus in the equation (13)

$$[\theta(x_0 - y_0) - \theta(y_0 - x_0)] \rightarrow \frac{1}{i\pi} \oint \frac{1}{\tau} e^{i\tau(x_0 - y_0)}$$

and it is responsible for the appearance of the dispersive integral as well as of the appearance of τ into energy momentum conservation δ functions.

7 Appendix B

We shall now explicitly verify Eqn. (7). We have

$$\begin{aligned}
(1/i^3)\tilde{G}(x, y, z) &= i^3 \Delta_{xy} \Delta_{yz} \Delta_{zx} = \theta_{xy} \theta_{yz} \Delta_{xy}^+ \Delta_{yz}^+ \Delta_{xz}^+ + \theta_{xy} \theta_{zx} \Delta_{xy}^+ \Delta_{zy}^+ \Delta_{zx}^+ \\
&\quad + \theta_{zy} \theta_{xz} \Delta_{xy}^+ \Delta_{zy}^+ \Delta_{xz}^+ + \theta_{yx} \theta_{xz} \Delta_{yx}^+ \Delta_{yz}^+ \Delta_{xz}^+ \\
&\quad + \theta_{yz} \theta_{zx} \Delta_{yx}^+ \Delta_{yz}^+ \Delta_{zx}^+ + \theta_{yx} \theta_{zy} \Delta_{yx}^+ \Delta_{zy}^+ \Delta_{zx}^+ \\
&= \theta_{xy} \theta_{yz} \Delta_{xy}^+ \Delta_{yz}^+ \Delta_{xz}^+ + \theta_{xy} \theta_{zx} \Delta_{xy}^+ \Delta_{zy}^+ \Delta_{zx}^+ \\
&\quad + \Delta_{xy}^+ \Delta_{zy}^+ \Delta_{xz}^+ - \theta_{yz} \Delta_{xy}^+ \Delta_{zy}^+ \Delta_{xz}^+ \\
&\quad - \theta_{zx} \Delta_{xy}^+ \Delta_{zy}^+ \Delta_{xz}^+ + \theta_{yz} \theta_{zx} \Delta_{xy}^+ \Delta_{zy}^+ \Delta_{xz}^+ \\
&\quad + \Delta_{yx}^+ \Delta_{yz}^+ \Delta_{xz}^+ - \theta_{xy} \Delta_{yx}^+ \Delta_{yz}^+ \Delta_{xz}^+ \\
&\quad - \theta_{zx} \Delta_{yx}^+ \Delta_{yz}^+ \Delta_{xz}^+ + \theta_{xy} \theta_{zx} \Delta_{yx}^+ \Delta_{yz}^+ \Delta_{xz}^+ \\
&\quad + \theta_{yz} \theta_{zx} \Delta_{yx}^+ \Delta_{yz}^+ \Delta_{zx}^+ + \Delta_{yx}^+ \Delta_{zy}^+ \Delta_{zx}^+ - \theta_{xy} \Delta_{yx}^+ \Delta_{zy}^+ \Delta_{zx}^+ \\
&\quad - \theta_{yz} \Delta_{yx}^+ \Delta_{zy}^+ \Delta_{zx}^+ + \theta_{xy} \theta_{yz} \Delta_{yx}^+ \Delta_{zy}^+ \Delta_{zx}^+ \\
&= \Delta_{xy}^+ \Delta_{zy}^+ \Delta_{xz}^+ + \Delta_{yx}^+ \Delta_{yz}^+ \Delta_{xz}^+ + \Delta_{yx}^+ \Delta_{zy}^+ \Delta_{zx}^+ \\
&\quad - \theta_{yz} \left(\Delta_{xy}^+ \Delta_{zy}^+ \Delta_{xz}^+ + \Delta_{yx}^+ \Delta_{zy}^+ \Delta_{zx}^+ \right) \\
&\quad - \theta_{zx} \left(\Delta_{xy}^+ \Delta_{zy}^+ \Delta_{xz}^+ + \Delta_{yx}^+ \Delta_{yz}^+ \Delta_{xz}^+ \right) \\
&\quad - \theta_{xy} \left(\Delta_{yx}^+ \Delta_{yz}^+ \Delta_{xz}^+ + \Delta_{yx}^+ \Delta_{zy}^+ \Delta_{zx}^+ \right) \\
&\quad + \theta_{xy} \theta_{yz} \left(\Delta_{xy}^+ \Delta_{yz}^+ \Delta_{xz}^+ + \Delta_{yx}^+ \Delta_{zy}^+ \Delta_{zx}^+ \right) \\
&\quad + \theta_{xy} \theta_{zx} \left(\Delta_{xy}^+ \Delta_{zy}^+ \Delta_{zx}^+ + \Delta_{yx}^+ \Delta_{yz}^+ \Delta_{xz}^+ \right) \\
&\quad + \theta_{yz} \theta_{zx} \left(\Delta_{xy}^+ \Delta_{zy}^+ \Delta_{xz}^+ + \Delta_{yx}^+ \Delta_{yz}^+ \Delta_{zx}^+ \right)
\end{aligned}$$

where $\theta_{AB} = \theta(A_0 - B_0)$ and we have repeatedly used $\theta_{AB} = 1 - \theta_{BA}$

Analogously we have

$$\begin{aligned}
(1/i^3)\tilde{G}(\underline{x}, y, z) &= \theta_{yz} \left(\Delta_{yx}^+ \Delta_{zx}^+ \Delta_{zy}^+ - \Delta_{yx}^+ \Delta_{zx}^+ \Delta_{yz}^+ \right) - \Delta_{yx}^+ \Delta_{zx}^+ \Delta_{zy}^+ \\
(1/i^3)\tilde{G}(x, \underline{y}, z) &= \theta_{zx} \left(\Delta_{xy}^+ \Delta_{zy}^+ \Delta_{xz}^+ - \Delta_{xy}^+ \Delta_{zy}^+ \Delta_{zx}^+ \right) - \Delta_{xy}^+ \Delta_{zy}^+ \Delta_{xz}^+ \\
(1/i^3)\tilde{G}(x, y, \underline{z}) &= \theta_{xy} \left(\Delta_{xz}^+ \Delta_{yz}^+ \Delta_{yx}^+ - \Delta_{xz}^+ \Delta_{yz}^+ \Delta_{xy}^+ \right) - \Delta_{xz}^+ \Delta_{yz}^+ \Delta_{yx}^+ \\
(1/i^3)\tilde{G}(x, \underline{y}, \underline{z}) &= \theta_{yz} \left(\Delta_{xy}^+ \Delta_{xz}^+ \Delta_{yz}^+ - \Delta_{xy}^+ \Delta_{xz}^+ \Delta_{zy}^+ \right) + \Delta_{xy}^+ \Delta_{xz}^+ \Delta_{zy}^+ \\
(1/i^3)\tilde{G}(\underline{x}, y, \underline{z}) &= \theta_{xz} \left(\Delta_{yx}^+ \Delta_{zy}^+ \Delta_{xz}^+ - \Delta_{yx}^+ \Delta_{zy}^+ \Delta_{zx}^+ \right) + \Delta_{yx}^+ \Delta_{zy}^+ \Delta_{xz}^+ \\
(1/i^3)\tilde{G}(\underline{x}, \underline{y}, z) &= \theta_{xy} \left(\Delta_{xz}^+ \Delta_{yz}^+ \Delta_{xy}^+ - \Delta_{xz}^+ \Delta_{yz}^+ \Delta_{yx}^+ \right) + \Delta_{xz}^+ \Delta_{yz}^+ \Delta_{yx}^+ \\
(1/i^3)\tilde{G}(\underline{x}, \underline{y}, \underline{z}) &= \Delta_{yx}^+ \Delta_{yz}^+ \Delta_{zx}^+ - \Delta_{xy}^+ \Delta_{zy}^+ \Delta_{zx}^+ - \Delta_{xy}^+ \Delta_{yz}^+ \Delta_{xz}^+
\end{aligned}$$

$$\begin{aligned}
& +\theta_{yz} \left(\Delta_{yx}^+ \Delta_{yz}^+ \Delta_{zx}^+ + \Delta_{xy}^+ \Delta_{yz}^+ \Delta_{xz}^+ \right) \\
& +\theta_{zx} \left(\Delta_{yx}^+ \Delta_{yz}^+ \Delta_{zx}^+ + \Delta_{xy}^+ \Delta_{zy}^+ \Delta_{zx}^+ \right) \\
& +\theta_{xy} \left(\Delta_{xy}^+ \Delta_{zy}^+ \Delta_{zx}^+ + \Delta_{xy}^+ \Delta_{yz}^+ \Delta_{xz}^+ \right) \\
& -\theta_{xy}\theta_{yz} \left(\Delta_{xy}^+ \Delta_{yz}^+ \Delta_{xz}^+ + \Delta_{yx}^+ \Delta_{zy}^+ \Delta_{zx}^+ \right) \\
& -\theta_{xy}\theta_{zx} \left(\Delta_{xy}^+ \Delta_{zy}^+ \Delta_{zx}^+ + \Delta_{yx}^+ \Delta_{yz}^+ \Delta_{xz}^+ \right) \\
& -\theta_{yz}\theta_{zx} \left(\Delta_{xy}^+ \Delta_{zy}^+ \Delta_{xz}^+ + \Delta_{yx}^+ \Delta_{yz}^+ \Delta_{zx}^+ \right)
\end{aligned} \tag{36}$$

and from Eqns. (36,36) we indeed obtain Eqn.(7).

References

- [1] M.L. Mangano, M. Moretti, F. Piccinini, R. Pittau and A.D. Polosa, JHEP **0307** (2003) 001.
- [2] A. Kanaki and C.G. Papadopoulos, Comput. Phys. Commun. **132** (2000) 306, [arXiv:hep-ph/0002082]; C.G. Papadopoulos and M. Worek, Eur. Phys. J. **C50** (2007) 843, [arXiv:hep-ph/0512150]; A. Cafarella, C.G. Papadopoulos and M. Worek, arXiv:0710.2427 [hep-ph].
- [3] T. Stelzer and W.F. Long, Comput. Phys. Commun. **81** (1994) 357, [arXiv:hep-ph/9401258]; F. Maltoni and T. Stelzer, JHEP **02** (2003) 027, [arXiv:hep-ph/0208156].
- [4] T. Gleisberg, S. Höche, F. Krauss, A. Schälicke, S. Schumann and J. Winter, , JHEP 0402 (2004) 056, [arXiv:hep-ph/0311263].
- [5] H. Murayama, I. Watanabe and K. Hagiwara, “Helas: Helicity amplitude subroutines for Feynman diagram evaluations”, KEK-91-11 (1992).
- [6] F. Caravaglios, M. Moretti, Phys. Lett. **B358** (1995) 332.
- [7] F. Caravaglios, M.L. Mangano, M. Moretti and R. Pittau, Nucl. Phys. **B539** (1999) 215.
- [8] A. Lazopoulos, K. Melnikov and F. Petriello, Phys. Rev. **D76** (2007) 014001, [arXiv:hep-ph/0703273]; V. Hankele and D. Zeppenfeld, arXiv:0712.3544 [hep-ph]; T. Plehn and M. Rauch, Phys. Rev. **D72** (2005) 053008, [arXiv:hep-ph/0507321]; T. Binoth, S. Karg, N. Kauer and R. Ruckl, Phys. Rev. **D74** (2006) 113008, [arXiv:hep-ph/0608057].
- [9] J.M. Campbell, R.K. Ellis and G. Zanderighi, JHEP **0610** (2006) 028, [arXiv:hep-ph/0608194]; M.M. Weber, Nucl. Phys. Proc. Suppl. **160** (2006) 200.
- [10] S. Dittmaier, P. Uwer and S. Weinzierl, Phys. Rev. Lett. **98** (2007) 262002, [arXiv:hep-ph/0703120].

- [11] B. Jager, C. Oleari and D. Zeppenfeld, JHEP **0607** (2006) 015, [arXiv:hep-ph/060317].
- [12] G. Bozzi, B. Jager, C. Oleari and D. Zeppenfeld, Phys. Rev. **D75** (2007) 073004;
- [13] A. Denner, S. Dittmaier, M. Roth and L.H. Wieders, Phys. Lett. **B612** (2005) 223, [arXiv:hep-ph/0502063]; A. Denner, S. Dittmaier, M. Roth and L.H. Wieders, Nucl. Phys. **B724** (2005) 247, [arXiv:hep-ph/0505042].
- [14] W.T. Giele and E.W.N. Glover, JHEP **0404** (2004) 029, [arXiv:hep-ph/0402152]; A. Denner and S. Dittmaier, Nucl. Phys. **B734** (2006) 105004, [arXiv:hep-ph/0602178].
- [15] R.K. Ellis, W.T. Giele and G. Zanderighi, JHEP **05** (2006) 027, [arXiv:hep-ph/0602185].
- [16] G. Mahlon, Phys. Rev. **D49** (1994) 2197, [arXiv:hep-ph/9311213]; arXiv:hep-ph/9412350; Z. Nagy and D.E. Soper, Phys. Rev. **D74** (2006) 093006, arXiv:hep-ph/0610028; G. Ossola, C.G. Papadopoulos and R. Pittau, JHEP **0707** (2007) 085, arXiv:0704.1271 [hep-ph]; T. Binoth, T. Gehrmann, G. Heinrich and P. Mastrolia, Phys. Lett. **B649** (2007) 422, arXiv:hep-ph/0703311.
- [17] A. Ferroglia, M. Passera, G. Passarino and S. Uccirati, Nucl. Phys. **B650** (2003) 162, arXiv:hep-ph/0209219.
- [18] G. Passarino, Nucl. Phys. **bf B619** (2001) 257, arXiv:hep-ph/0108252.
- [19] S. Actis and G. Passarino, Nucl. Phys. **B777** (2007) 100, hep-ph/0612124; Nucl. Phys. **B777** (2007) 35, hep-ph/0612123; S. Actis, A. Ferroglia, M. Passera and G. Passarino, Nucl. Phys. **B777** (2007) 1.
- [20] Z. Nagy and D.E. Soper, JHEP **0309** (2003) 055, [arXiv:hep-ph/0308127]; Acta Phys. Polon. **B35** (2004) 2557; M. Kramer and D.E. Soper, Phys. Rev. **D66** (2002) 054017, [arXiv:hep-ph/0204113]; D.E. Soper, Phys. Rev. Lett. **81** (1998) 2638, [arXiv:hep-ph/9804454]; Phys. Rev. **D62** (2000) 014009, [arXiv:hep-ph/9910292]; Phys. Rev. **D64** (2001) 034018, [arXiv:hep-ph/0103262].
- [21] Z. Bern, L.J. Dixon, D.A. Kosower, Ann. Phys. **322** (2007) 1587, arXiv:0704.2798 [hep-ph].
- [22] G. Ossola, C.G. Papadopoulos and R. Pittau, Nucl. Phys. **B763** (2007) 147 [arXiv:hep-ph/0609007]; JHEP **0707** (2007) 085, [arXiv:0704.1271 [hep-ph]]; arXiv:0711.3596 [hep-ph].
- [23] T. Binoth, J.P. Guillet, G. Heinrich, E. Pilon and C. Schubert, JHEP **0510** (2005) 015, [arXiv:hep-ph/0504267]; T. Binoth, J.P. Guillet and G. Heinrich, JHEP **0702** (2007) 013, [arXiv:hep-ph/0609054]; Z.G. Xiao, C. Yang and C.J. Zhu, Nucl. Phys. **B758** (2006) 1, [arXiv:hep-ph/0607015]; X. Su, Z.G. Xiao, C. Yang and C.J. Zhu, Nucl. Phys. **B758** (2006) 35, [arXiv:hep-ph/0607016]; Z. Bern, L.J. Dixon and D.A. Kosower, Phys. Rev. **D73** (2006) 065013,

- [arXiv:hep-ph/0507005]; S.D. Badger, E.W.N. Glover and K. Risager, JHEP **0707** (2007) 066, [arXiv:0704.3914[hep-ph]]; C.F. Berger, Z. Bern, L.J. Dixon, D. Forde and D.A. Kosower, Phys. Rev. **D75** (2007) 016006, [arXiv:hep-ph/0607014]; C. Anastasiou, R. Britto, B. Feng, Z. Kunszt and P. Mastrolia, Phys. Lett. **B645** (2007) 213 [arXiv:hep-ph/0609191]; JHEP **0703** (2007) 111; R. Britto and B. Feng, arXiv:hep-ph/07114284.
- [24] W.T. Giele, Z. Kunszt and K. Melnikov, arXiv:0801.2237 [hep-ph].
- [25] M.J. Veltman, “Dispersive calculation of diagrams with arbitrarily external legs”, in, “Colloquium on Advanced Computing Methods in Theoretical Physics”, vol. 2, pag. IV-115, Marseille, 21-25 June 1971;
- [26] G.’t Hooft and M.J. Veltman, “Diagrammar,” CERN Report 73-79, 1973, published in NATO Adv. Study Inst. Ser. B Phys. 4 p. 177-322, 1974
- [27] M. Bonini, M. D’Attanasio, G. Marchesini, Nucl. Phys. **B444** (1995) 602.
- [28] G. Passarino and M.J. Veltman, Nucl. Phys. **B160** (1979) 151; G.’t Hooft and M.J. Veltman, Nucl. Phys. **B153** (1979) 365.
- [29] T. Hahn and M. Perez-Victoria, Comput. Phys. Commun. **118** (1999) 153.